ANALYSIS OF OVERESTIMATION IN HISTORICAL ICE FLOW VELOCITY MAPS IN WESTERN PACIFIC OCEAN SECTOR, ANTARCTICA

S. Ge[1,2], Y. Cheng[1,2] *, R. Li[1,2] *, H. Cui[1,2], Z. Yu[1,2], T. Chang[1,2], S. Luo[1,2], Z. Li[1,2], G. Li[1,2], A. Zhao[1,2],
X. Yuan[1,2], Y. Li[1,2], M. Xia[1,2], X. Wang[1,2], G. Qiao[1,2] *

[1]Center for Spatial Information Science and Sustainable Development Applications, Tongji University, 1239 Siping Road, Shanghai
200092, China – (geshaocang, chengyuan_1994, rli, haotiancui, yuzeran, ctzry, shulei, genlee, liguojunlee, zhaoaiguo,
1996yuanxiaohan, 1710992, menglianxia, wxfjj620, qiaogang)@tongji.edu.cn
[2]College of Surveying and Geo-Informatics, Tongji University, 1239 Siping Road, Shanghai, China

Commission TCIII, WG III/9

KEY WORDS: Adjustment, Overestimation, Historical Ice Velocity, Acceleration, East Antarctica.

ABSTRACT:

High accuracy reconstruction of historical ice flow velocity fields is crucial in mass balance research of the Antarctic Ice Sheet by utilizing the input-output approach. A historical flow velocity of the Western Pacific Ocean sector region of East Antarctica from 1963 to 1989 was mapped and then corrected for its velocity overestimation. In this study, we analyzed the spatial distribution of the corrected values, and further assessed the relationship between the corrected values and related factors including timespan of image pairs, ice flow velocity, the spatial acceleration of ice flow velocity, and surface slope. The results indicate that the corrected ice flow velocity points are mostly dispersed between a buffer 25 km upstream and a buffer 25 km downstream the grounding line, with the largest mean value emerging in the region between the grounding line and its 25 km downstream. The corrected values exhibit linear correlation with three conditions: 1) when the ice flow velocity range is $0 \sim 1586$ m/y, 2) spatial acceleration is $0 \sim 69$ (m/y)/km, and 3) the slope is $0 \sim 1.95$ degrees and the R^2 is higher than 0.7. However, the correlation between timespan and corrected values is not obvious. The corrected values for the floating region have a greater linear correlation with all three factors than the inland region. Ice flow velocity, spatial acceleration, and surface slope all have an influence on the distribution of the corrected values of the reconstructed historical ice flow velocity maps, and may further affect the assessment of the mass balance of the Antarctic Ice Sheet.

1. INTRODUCTION

Antarctic Ice Sheet (AIS) holds the majority of the earth's fresh water, ~91% of the global ice mass. The ice mass loss of the AIS directly impacts the amplitude of the sea level rise (Shepherd et al., 2012; Rignot et al., 2019; Bell et al., 2020; Dirscherl et al., 2020). The total ice volume of the AIS can contribute ~58 m to sea level rise (Fretwell et al., 2013; Morlighem et al., 2020). AIS gains mass from precipitation and loses mass by solid ice discharging to the ocean (more than 90%) and other processes such as sublimation, wind-driven snow transport, meltwater runoff and basal melt (Gardner et al., 2018). Ice flow velocity plays an important role in evaluating the ice discharge from the AIS to the Southern Ocean via the input-output method (Shepherd et al., 2012; Gardner et al., 2018; IMBIE, 2018; Shen et al., 2018; Rignot et al., 2019). Thus, it is necessary to reconstruct the ice flow velocity maps with high precision and accuracy.

The existing ice flow velocity products covering the AIS include MEaSUREs (Rignot et al., 2011; Mouginot et al., 2017), ITS-LIVE (Gardner et al., 2018) and Landsat-8 velocity maps (Shen et al., 2021), etc. However, the large-scale historical velocity of Antarctica has not been well studied yet. More importantly, the scarcity of historical images and long time span of image pair may lead to the overestimation of ice flow velocity (Li et al., 2022). An innovative Lagrangian velocity-based method is proposed to solved this problem (Li et al., 2022). The Western Pacific Ocean sector of the AIS (Parkinson 2019), especially the Wilkes Land, has the highest and accelerating mass loss in East

Antarctica (Shen et al, 2018; Rignot et al., 2019). In recent years, the activity of Circumpolar Deep Water (CDW) in this area has attracted a widespread concern, which may be related to the acceleration of regional mass loss (Adusumilli et al., 2020).

We have previously mapped the historical ice velocity by using ARGON, Landsat-1, 4 and 5 images spanning from 1963 to 1989, in the Western Pacific Ocean sector region of East Antarctica (Cheng et al., 2019; Luo et al., 2021), and corrected the overestimation in velocity based on the Lagrangian velocity-based method (Li et al., 2022). In this study, we assess the magnitude and spatial distribution of the corrected results (Figure 2). Furthermore, we analyse the relationship between the corrected values and the influencing factors such as the time span, topography and slope of the study area, and spatial acceleration. We find that these factors may impact the distribution of the corrected values of the reconstructed historical ice flow velocity maps.

2. DATA AND METHODS

2.1 Study Area and Data

The Western Pacific Ocean sector of AIS (090° E-160°E; Figure 1; Parkinson 2019) mainly consists of Queen Mary Land (091°54' E-100°30' E), Wilkes Land (100°31' E-136°11' E), Adélie Land (136°11′E, 142°02′E), George V Land (142°02' E, 153°45' E) and Oates Land (153°45' E, 160°00' E). The main outlets of mass in the sector include Denman Glacier, Totten Glacier, Moscow

---
* Corresponding author

University Ice Shelf, Frost Glacier, Dibble Glacier, Mertz Ice Shelf, Ninnis Ice Shelf and Cook Ice Shelf.
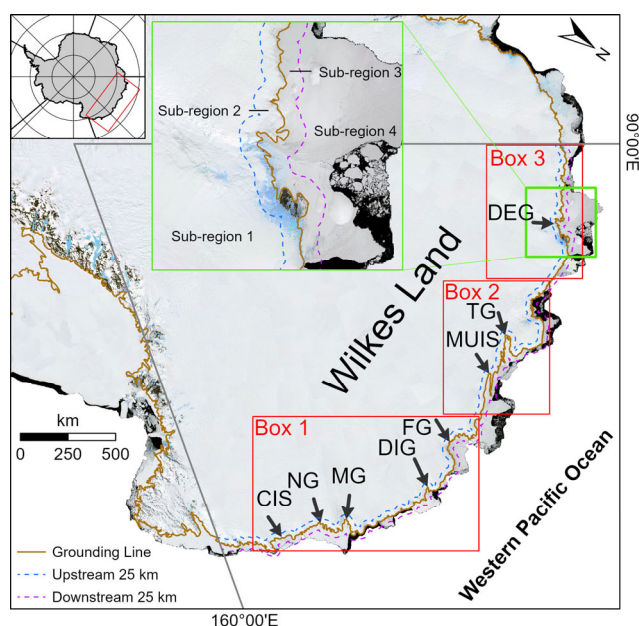

Figure 1. The location of the Western Pacific Ocean sector region of East Antarctica. The background is the LIMA mosaic (Bindschadler et al., 2008). The brown line is the grounding line (GL) (Gardner et al., 2018). DEG denotes the Denman Glacier, TG the Totten Glacier, MUIS the Moscow University Ice shelf, FG the Frost Glacier, DIG the Dibble Glacier, MG the Mertz Glacier, NG the Ninnis Glacier, CIS the Cook Ice Shelf. The red boxes represent the three regions of Figure 2. The inset is an enlarged view of the green box, displaying an example of sub-regions 1-4 to reveal the spatial distribution of the corrected values.

Historical ice flow velocity from 1963 to 1989 is extracted from ARGON and Landsat 1, 4 and 5 images by using feature tracking. All historical images are orthorectified with geographical reference of LIMA (Bindschadler et al., 2008). The positioning and matching accuracy of most image pairs are within one pixel. The main purpose of this paper is to correct and analyse the distribution and impact factors of the corrected values of the historical ice flow velocity in the Western Pacific Ocean sector of Antarctica. The experiment is carried out at the ice flow velocity points, that is, the matched points from image pairs. REMA DEM is an Antarctic DEM product reconstructed from worldview-1, worldview-2, worldview-3 and GeoEye-1 images with an absolute uncertainty within 1 m. This high-precision makes it sufficient to calculate the slope of the ice surface.

2.2 Methods

An innovative Lagrangian velocity-based method is employed by Li et al. (2022) for overestimation correction: the velocity calculated by feature matching of the image pair with a time interval of n years is the Euler velocity (E-v), and the ice flow trajectory tracking for n years on the velocity map is used to obtain the Lagrange velocity (L-v); the difference between the E-v and L-v is regarded as the velocity overestimation and is applied to correct the ice flow velocity. In this study, we only counted the correction values above 10 m/y and ignored those below 10 m/y.

To reveal the spatial distribution of the corrected values, the study area is divided into four sub-regions (Figure 1): sub-region 1 is from inland to 25 km upstream GL; sub-region 2 is from 25 km upstream GL to GL; sub-region 3 is from GL to 25 km downstream GL and sub-region 4 is from 25 km downstream GL to the front of ice shelf or glacier. Meanwhile, several statistical analyses are conducted to investigate factors that may affect the corrected values, including ice flow velocity, the acceleration of ice flow velocity field, surface slope and the timespan of the image pairs used to generate the ice flow velocity maps. The relationship between the corrected values and these factors are also analyzed and discussed. The spatial acceleration of ice flow velocity field was calculated in 2 km range along the direction of ice flow. The surface slope was extracted from REMA DEM product with a resolution of 200 m and average in a range of 1km × 1km.

3. RESULTS AND DISCUSSION

3.1 Quantitive analysis of overestimation

Totally 18,293 ice flow velocity points with overestimation over 10 m/y in the Western Pacific Ocean sector of AIS were analysed. For all points, the mean ice flow velocity is ~600 m/y, with a mean corrected value of ~-56 m/y, which accounts for ~10.6% of the average ice flow velocity.

As shown in Figures 2 and 3, the points need to be corrected are mostly distributed within 25 km upstream and 25 km downstream of the GL, with ~27.8% (5,091 points) in sub-region 2 and ~57.8% (10,566 points) in sub-region 3. Points of sub-region 1 and sub-region 4 accounted for only ~13.6% and ~0.8%, respectively. Sub-region 3 has the largest mean corrected value of ~-75 m/y, with a standard deviation of ~61 m/y. The averaged ice flow velocity in this region is ~829 m/y, and the ice flow velocity overestimation accounts for ~8.9%, which indicates the necessity of correction. The sub-region 2 is followed with a corrected value of ~-36 m/y. The smallest corrected value is in sub-region1, ~-23 m/y. The corrected value accounts for ~10.3%, indicating no obvious overestimation in sub-region 1.
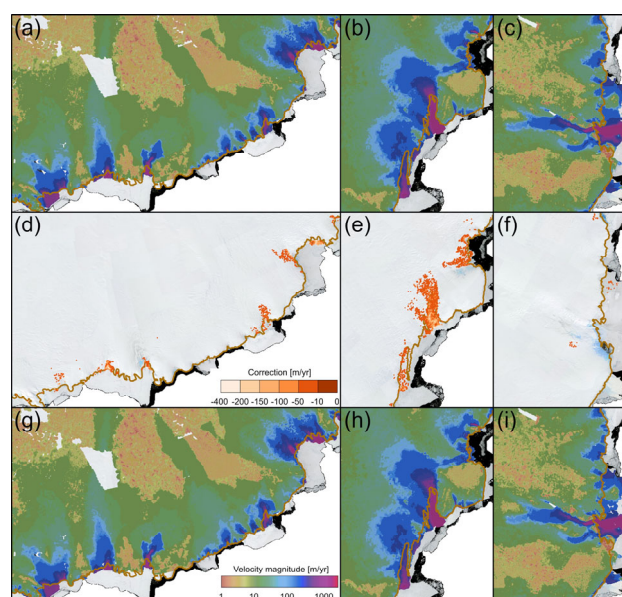

Figure 2. (a), (b), and (c) are the corresponding historical ice flow velocity maps of Boxes 1-3 in Figure 1 before correction. (d), (e), and (f) are the distributions of the corrected values in Boxes 1-3. (g), (h), and (i) are the corresponding historical ice flow velocity maps after correction.
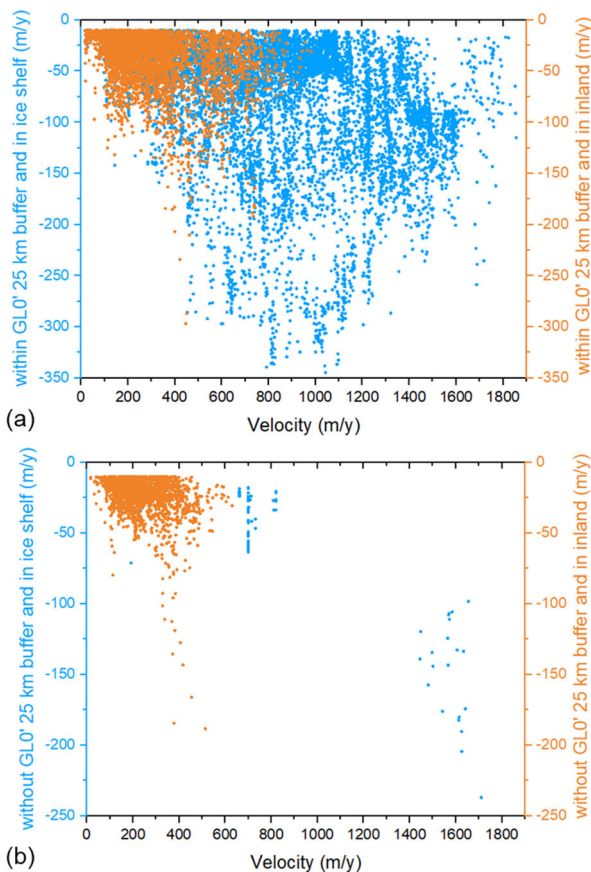
Figure 3. The distribution of the corrected values (a) within GL0'25 km buffer and (b) without GL0'25 km buffer, the blue dots represent the corrected values in ice shelf and the orange dots represent the corrected values in inland.

3.2 Relationship between the corrected values and factors

Figures 4-7 show the relationship between corrected values and related factors, including timespan of image pairs (Figure 4), ice flow velocity (V; Figure 5), spatial acceleration of ice flow velocity (AV; Figure 6) and surface slope (Figure 7). Among the Figures 4 to 7, figures in four columns (a-d) represent the results of four sub-regions. For Figures 4-7, the first row of each figure are the count of the corrected ice flow velocity points vs. factors including timespan of image pairs (Figure 4), V (Figure 5), AV (Figure 6) and surface slope (Figure 7) for 4 sub-regions; figures in the second row present the change of the corrected values with respect to the factors; each figure in the third row corresponds to an enlarged display of the red part of the second row, which also present the correlation between the corrected values and each factor. In addition, the red part in second row of Figures 4-7 represents there is a linear correlation between the corrected values and the factor, the grey part represents there is no linear or other trend between the corrected values and the factor, which will not be explored in this study since there are too few data points.

For the entire region, ~99% points (0 ~ 1586 m/y) show an obvious linear correlation between the corrected values and V. For corrected values and AV, ~93% points exhibit linear relationship with AV in 0 ~ 69 (m/y)/km. The number of points with surface slope in 0 ~ 1.9 degrees is linearly related to the corrected values, accounting for ~88% of the total numbers of points. This reveals that at most points, the corrected values are linearly correlated with ice flow velocity, spatial acceleration, and slope with $R^2 > 0.7$. There is no linear or other trend in the correction values when the V exceeds 1586 m/y, or the AV exceeds 69 (m/y)/km, or the slope exceeds 1.9 degrees (the grey bars of histogram in Figure 4-7). It will not be explored here since there are too few points. In terms of timespan, there is no discernible pattern, whether linear or otherwise. Despite the fact that the results reveal no evident correlation between the timespan and the corrected values, the long-time interval is still a significant cause of overestimation.

It is considered that whether the ice is grounded or not has a significant impact on its assessment. The relationship between the corrected values and the factors is also analysed on the upstream and downstream of the GL. The points of the upstream of the GL (inland region) and the downstream of the GL (floating region) are 7579 (~41.4%) and 10704 (~58.6%), respectively. Further, we also make a comparative analysis on the four sub-regions. Among them, the points of sub-region 4 only account for ~0.8% (148), which will not be discussed in detail here (Figure 4-7d). For inland regions (sub-region 1 and 2) the relationship between the corrected values and AV of the inland region is similar to that of the entire region, and is linearly correlated to the corrected value with ~92% points (Figure6(a, b)). However, the linear relationship between corrected values and V weakens, with just ~87% of the points exhibiting a linear trend (Figure 5(a, b)). The linear correlation between the corrected values and slope shows a low R^2 of ~0.3 (Figure 7(a, b)), indicating that the slope has little influence on the corrected value in inland region. In details, the points in sub-region 1 and 2 are 2488 (~13.6%) and 5091 (~27.8%), respectively. The relationships between the corrected values and these factors show relatively inconsistent in this two sub-regions. The fitting R^2 between corrected values and slope is ~0.7 in sub-region 1, but only ~0.3 in sub-region 2. For the fitting R^2 of corrected values and AV, the sub-region 2 is ~0.63, but is only ~0.48 in sub-region 1. For the floating region (sub-region 3), the corrected values maintains a good linear correlation with V (Figure 5(c)), AV (Figure 6(c)) and slope (Figure 7(c)). Compared with the inland region, the points of the floating region with linear correlation on slope grow to ~95%, while those with linear correlation on acceleration decline to ~76%.
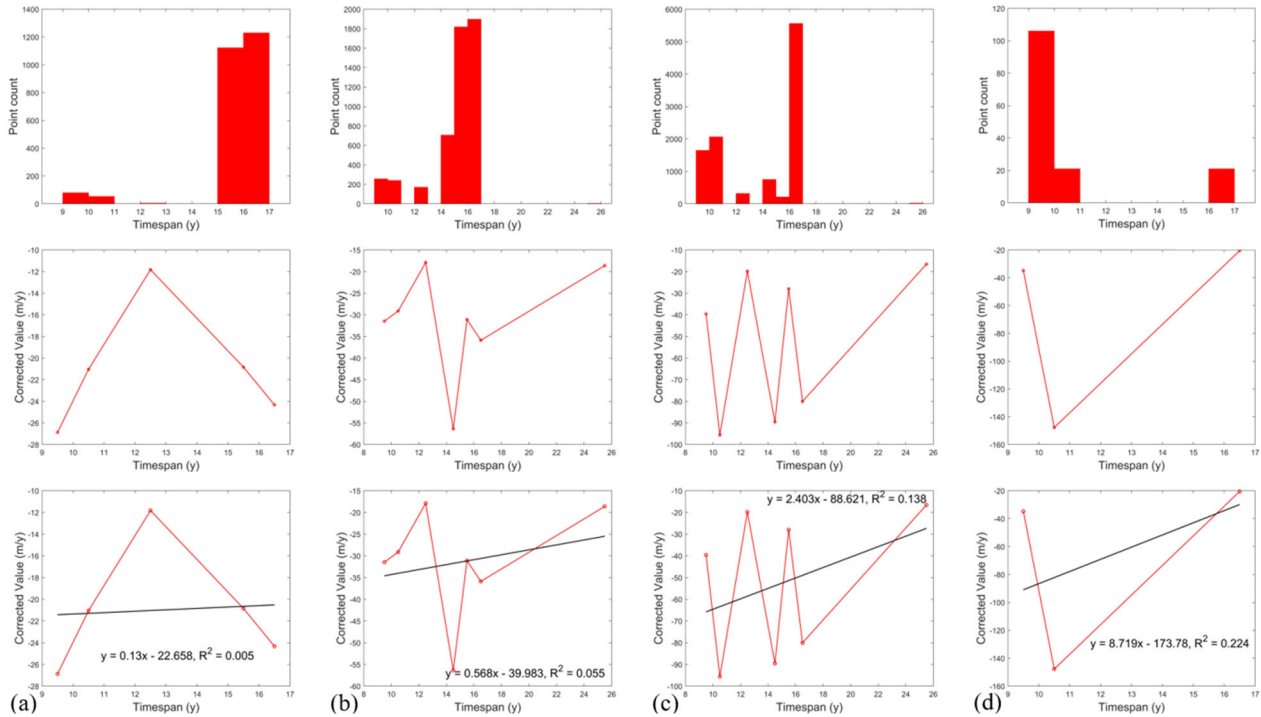
Figure 4. The relationship between corrected values and Timespan (a) without GL0'25 km buffer and in inland (Sub-region 1), (b) within GL0'25 km buffer and in inland (Sub-region 2), (c) within GL0'25 km buffer and in ice shelf (Sub-region 3), (d) without GL0'25 km buffer and in ice shelf (Sub-region 4).
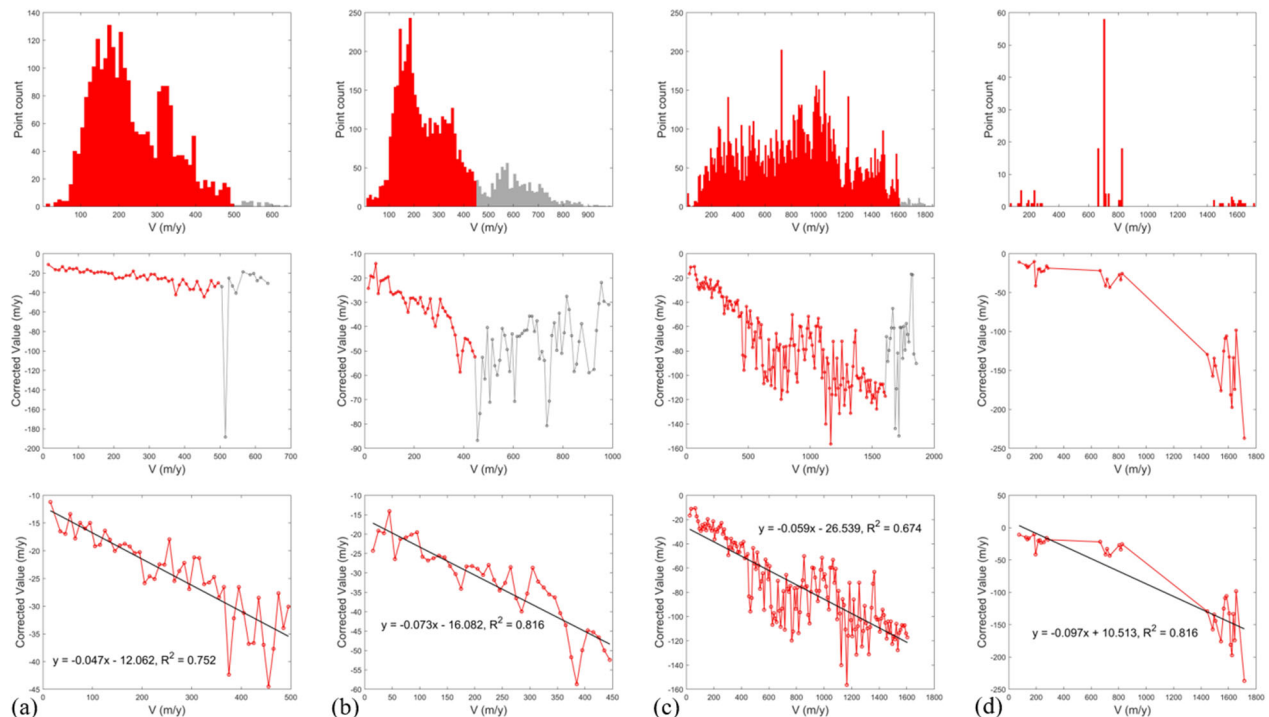

Figure 5. The relationship between corrected values and V (a) without GL0'25 km buffer and in inland (Sub-region 1), (b) within GL0'25 km buffer and in inland (Sub-region 2), (c) within GL0'25 km buffer and in ice shelf (Sub-region 3), (d) without GL0'25 km buffer and in ice shelf (Sub-region 4).
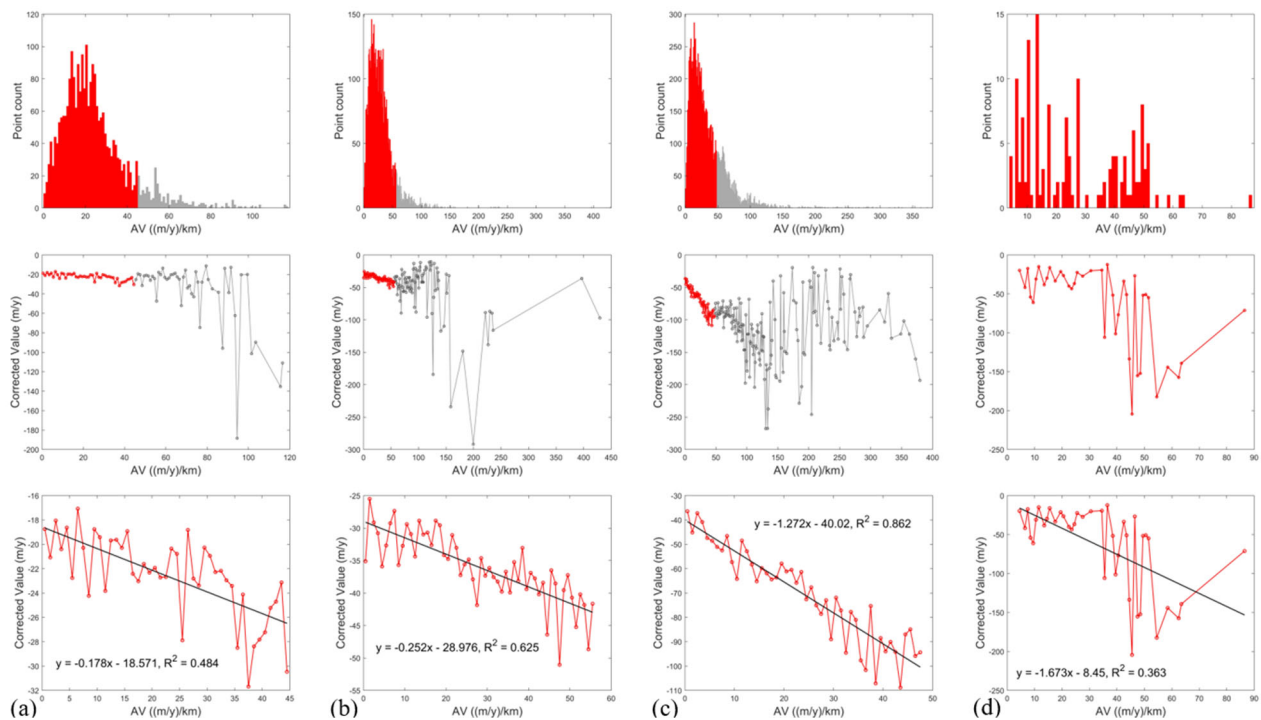
Figure 6. The relationship between corrected values and AV (a) without GL0'25 km buffer and in inland (Sub-region 1), (b) within GL0'25 km buffer and in inland (Sub-region 2), (c) within GL0'25 km buffer and in ice shelf (Sub-region 3), (d) without GL0'25 km buffer and in ice shelf (Sub-region 4).
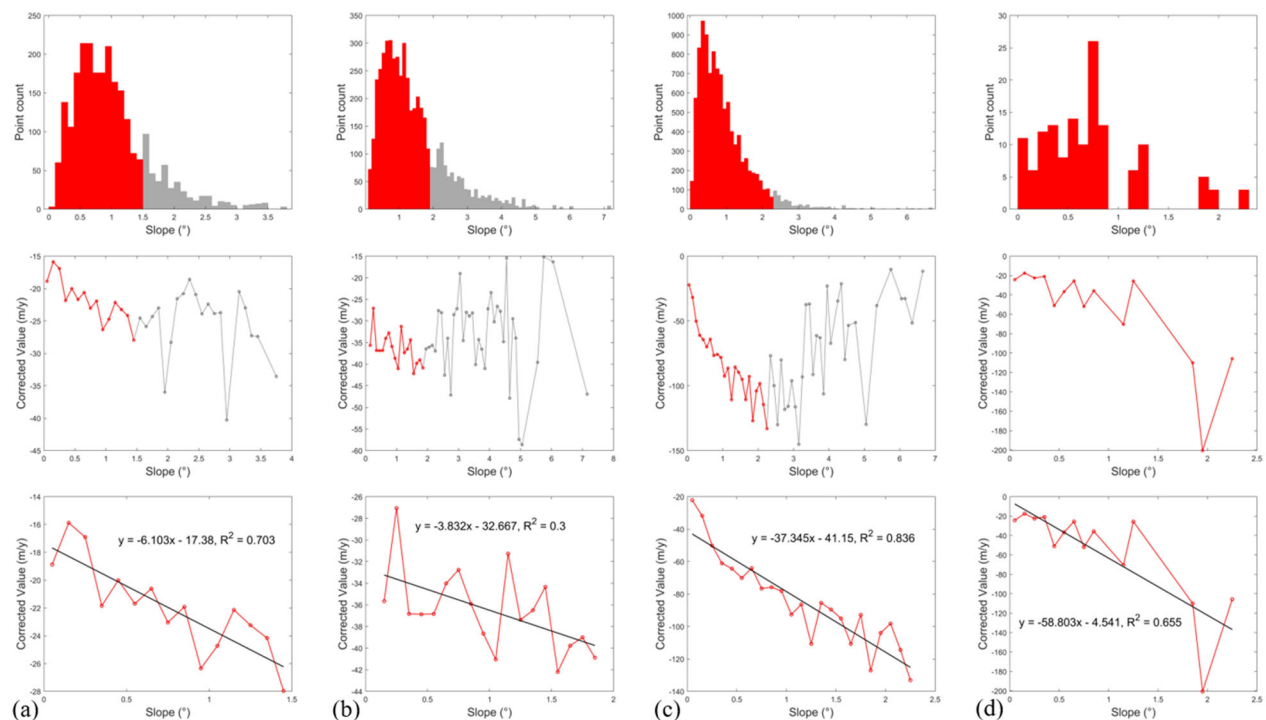

Figure 7. The relationship between corrected values and the slope of velocity field (a) without GL0'25 km buffer and in inland (Sub-region 1), (b) within GL0'25 km buffer and in inland (Sub-region 2), (c) within GL0'25 km buffer and in ice shelf (Sub-region 3), (d) without GL0'25 km buffer and in ice shelf (Sub-region 4).

4. CONCLUSIONS

In this study, we counted the velocity overestimation values of the historical ice flow velocity maps of the Western Pacific Ocean sector region of the East Antarctica spanning 1963 -1989, to analyse the spatial distribution of the corrected values and evaluate the relationship between corrected values and related factors including timespan of image pairs, ice flow velocity, the spatial acceleration of ice flow velocity and surface slope.

The results reflect that ~1.3% velocity points have been corrected in the Western Pacific Ocean sector of AIS. These points are mainly distributed within the buffer of 25 km upstream and downstream the grounding line, with the largest mean corrected values emerged in sub-region 3 and the smallest in sub-region 1, which has a great influence on the calculation of mass balance. When the ice flow velocity range is 0 ~ 1586 m/y, or the AV range is 0 ~ 69 (m/y)/km, or slope is 0 ~ 1.9 degrees, the corrected values show linear correlation with these three factors respectively, while the R^2 of all three factors are greater than 0.7. Although there is no obvious correlation between timespan and corrected values, a long time span is nevertheless a significant cause of overestimation and the issue needs a further analysis in other sectors. In the inland region, the linear relationship between corrected values and V (~87%) is weaker than the relationship between the corrected values and AV (~92%), and the linear correlation between the corrected values and slope shows a lower R^2. By contrast, the corrected values for the floating region maintains a good linear correlation with all these three factors. All of this suggests that the ice flow velocity, the spatial acceleration, and the surface slope can influence the distribution of the corrected values of the reconstructed historical ice flow velocity maps, and therefore the evaluation of mass balance in the local or even the entire AIS.

ACKNOWLEDGEMENTS

Author contributions: RL led the study and developed the overestimation correction model. YC is involved in method implementation and computed overestimation values, SG performed statistical analysis, HC performed programming. Everyone is involved in velocity mapping and map correction.

REFERENCES

Adusumilli, S., Fricker, H.A., Medley, B., Padman, L., Siegfried, M.R., 2020. Interannual variations in meltwater input to the Southern Ocean from Antarctic ice shelves. *Nature geoscience*, 13(9), 616-620.

Bell, R.E., Seroussi, H., 2020. History, mass loss, structure, and dynamic behavior of the Antarctic Ice Sheet. *Science*, 367(6484), 1321-1325.

Bindschadler, R., Vornberger, P., Fleming, A., Fox, A., Mullins, J., Binnie, D., Gorodetzky, D., 2008. The Landsat image mosaic of Antarctica. *Remote Sensing of Environment*, 112(12), 4214-4226.

Cheng, Y., Li, X., Qiao, G., Ye, W., Huang, Y., Li, Y., ... & Li, R., 2019. Ice Flow Velocity Mapping of East Antarctica from 1963 TO 1989. *The International Archives of Photogrammetry, Remote Sensing and Spatial Information Sciences*, 42, 1735-1739.

Dirscherl, M., Dietz, A.J., Dech, S., Kuenzer, C., 2020. Remote sensing of ice motion in Antarctica–A review. *Remote Sensing of Environment*, 237, 111595.

Fretwell, P., Pritchard, H.D., Vaughan, D.G., Bamber, J.L., Barrand, N.E., Bell, R., Zirizzotti, A., 2013. Bedmap2: improved ice bed, surface and thickness datasets for Antarctica. *The Cryosphere*, 7(1), 375-393.

Gardner, A.S., Moholdt, G., Scambos, T., Fahnstock, M., Ligtenberg, S., Broeke, M.V.D., Nilsson, J., 2018. Increased West Antarctic and unchanged East Antarctic ice discharge over the last 7 years. *The Cryosphere*, 12(2), 521-547.

IMBIE, 2018. Mass balance of the Antarctic Ice Sheet from 1992 to 2017. *Nature*, 558(7709), 219-222.

Li, R., Cheng, Y., Cui, H., 2022. Overestimation and adjustment of Antarctic ice flow velocity fields reconstructed from historical satellite imagery[J]. *The Cryosphere*, 2022, 16(2): 737-760.

Luo, S., Cheng, Y., Li, Z., Wang, Y., Wang, K., Wang, X., ... & Li, R., 2021. Ice Flow Velocity Mapping in East Antarctica Using Historical Images from 1960s to 1980s. Recent Progress. *The International Archives of Photogrammetry, Remote Sensing and Spatial Information Sciences*, 43, 491-496.

Morlighem, M., Rignot, E., Binder, T., Blankenship, D., Drews, R., Eagles, G., Young, D.A., 2020. Deep glacial troughs and stabilizing ridges unveiled beneath the margins of the Antarctic ice sheet. *Nature Geoscience*, 13(2), 132-137.

Mouginot. J, Rignot. E, Scheuchl. B and Millan. R., 2017. Comprehensive annual Ice Sheet velocity mapping using Landsat-8, Sentinel-1, and RADARSAT-2 Data. *Remote Sensing*, 9(4), 364.

Parkinson, C.L., 2019. A 40-y record reveals gradual Antarctic sea ice increases followed by decreases at rates far exceeding the rates seen in the Arctic. *Proceedings of the National Academy of Sciences*, 116(29), 14414-14423.

Rignot, E., Mouginot, J., Scheuchl, B., 2011. Ice flow of the Antarctic ice sheet. *Science*, 333(6048), 1427-1430.

Rignot, E., Mouginot, J., Scheuchl, B., Van den Broeke, M., Van Wessem, M., Morlighem, M., 2019. Four decades of Antarctic Ice Sheet mass balance from 1979–2017. *Proceedings of the National Academy of Sciences* 116, 1095–1103.

Shen, Q., Wang, H., Shum, C.K., Jiang, L., Hsu, H.T., Dong, J., 2018. Recent high-resolution Antarctic ice velocity maps reveal increased mass loss in Wilkes Land, East Antarctica, *Sci. Rep.-UK*, 8(1), 4477.

Shen, Q., Wang, H., Shum, C.K., Jiang, L., Hsu, H., Gao, F., Zhao, Y., 2021. Antarctic-wide annual ice flow maps from Landsat 8 imagery between 2013 and 2019. *International Journal of Digital Earth*, 14(5), 597-618.

Shepherd, A., Ivins, E.R., Barletta, V.R., Bentley, M.J., Bettadpur, S., Briggs, K.H., Bromwich, D.H., Forsberg, R., Galin, N., Horwath, M., Jacobs, S., Joughin, I., King, M.A., Jan, T.M.L., Li, J., Stefan, R.M.L., Luckman, A., Luthcke, S.B., McMillan, M., Meister, R., Milne, G., Mouginot, J., Muir, A., Nicolas, J.P., Paden, J., Payne, A.J., Pritchard, H., Rignot, E., Rott, H., Sørensen, L.S., Scambos, T.A., Scheuchl, B., Ernst, J.O.S., Smith, B., Sundal, A.V., Jan, H.V.A., Willem, J.V.D.B., Michiel, R.V.D.B., Vaughan, D.G., Velicogna, I., Wahr, J., Whitehouse, P.L., Wingham, D.J., Yi, D., Young, D., Zwally, H.J., 2012. A reconciled estimate of Ice-Sheet mass balance. *Science*, 338 (6111), 1183-1189.